ISIJ International, Advance Publication by J-STAGE, DOI: 10.2355/isijinternational.ISIJINT-2016-095

On Strengthening of Austenitic Stainless Steel by Large Strain Cold Working

Iaroslava SHAKHOVA,[1)] Andrey BELYAKOV,[1)]* Zhanna YANUSHKEVICH,[1)] Kaneaki TSUZAKI[2)] and Rustam KAIBYSHEV[1)]

1) Belgorod State University, Pobeda 85, Belgorod, 308015 Russia.
2) Kyushu University, Department of Mechanical Engineering, 744 Motooka, Nishi-ku, Fukuoka, 819-0395 Japan.

(*Received on February 16, 2016; accepted on March 11, 2016; J-STAGE Advance published date: June 7, 2016*)

The tensile properties of an S304H austenitic stainless steel processed by large strain cold rolling were studied. Cold rolling was accompanied by the deformation twinning and martensitic transformation. The fraction of strain-induced martensite comprised 0.65 after cold rolling to a total strain of 4. The transverse grain size progressively reduced to about 200 nm in both the austenite and martensite phases. The deformation microstructures were characterized by large internal distortions, which were attributed to high dislocation density well above 10^{15} m^{-2}. Cold rolling resulted in significant strengthening. The yield strength increased from 290 MPa in the initial annealed state to 2 050 MPa in the sample subjected to cold rolling to a total strain of 4. The strengthening could be adequately explained by increasing the dislocation density. In the framework of dislocation strengthening model the austenite and strain-induced martensite provided equal fractional contribution to the overall strength of the rolled steel.

KEY WORDS: austenitic stainless steel; cold rolling; strain-induced martensite; grain refinement; strengthening.

1. Introduction

Austenitic stainless steels are widely used engineering materials exhibiting a good workability and corrosion resistance.[1)] However, hot worked semi-products of austenitic stainless steels with recrystallized microstructures are characterized by a common disadvantage that is relatively low yield strength.[2)] This restricts certain applications, which require enhanced strength properties. The yield strength of austenitic stainless steels can be significantly increased by cold working, *i.e.*, plastic deformation at ambient temperature.[3–6)] Among various techniques of cold deformation, cold rolling is the most efficient method for production of the sizable semi-products of stainless steels. The cold rolling techniques have been successfully utilized for development of stainless steels with high yield strength above 1 500 MPa.[7–9)] However, the structural mechanisms responsible for such effective strengthening of austenitic stainless steels by cold working have not been studied in sufficient details.

Austenitic stainless steels are commonly characterized by relatively low stacking fault energy (SFE).[10–12)] Therefore, the deformation twinning frequently operates in these materials during cold working.[12)] Another feature of austenitic stainless steels subjected to cold working is the strain-induced martensitic transformation because the austenite in these steels is metastable at ambient temperature.[13–16)] The development of deformation twinning and strain-induced martensitic transformation during cold working results in rapid refinement of the steel microstructure. Stainless steels with grain/subgrain sizes of tens to hundreds nanometers have been obtained by using large strain cold deformations.[4,17,18)] In previous studies, the strengthening of austenitic stainless steels processed by severe plastic deformations was commonly attributed to the developed nanocrystalline structures.[4–9,18–20)] It should be noted, that the ultrafine grained microstructures that developed in stainless steels during cold deformation were characterized by high dislocation densities. The corresponding internal stresses could also affect the strength of the processed steels.[8)] However, the effect of internal stresses evolved in severely strained submicrocrystalline/nanocrystalline steels on the yield strength has not been clarified.

The aim of the present study is to clarify the relationship between the cold worked microstructure and strength of an austenitic stainless steel. The work is focused on the investigation of structural mechanisms responsible to the strengthening of the steel and the evaluation of their contributions to the yield strength.

2. Experimental

The starting material was an S304H-type austenitic stainless steel having chemical composition (weight percent) of Fe–0.1C–0.12N–0.1Si–0.95Mn–18.4Cr–7.85Ni–2.24Cu–0.5Nb–0.01P–0.006S. The steel rods with transverse section

* Corresponding author: E-mail: belyakov@bsu.edu.ru
DOI: http://dx.doi.org/10.2355/isijinternational.ISIJINT-2016-095

© 2016 ISIJ

of 20 × 20 mm^2 were hot rolled at 973 K and then annealed at 1 100°C for 10 min with subsequent water quenching. Then, the square bar samples with initial cross area of 9.2 × 9.2 mm^2 were square bar rolled to various total true strains ($\varepsilon = \ln S_0/S_\varepsilon$, where S_0 and S_ε are the initial cross area and that one after rolling, respectively) up to 4 at room temperature. The rolled bars were cooled by water after each 0.1 strain increment to avoid the temperature rise. Structural investigations were performed on sections parallel to the rolling axis using a Quanta 600 FEG scanning electron microscope equipped with an electron backscattering diffraction (EBSD) analyzer incorporating an orientation imaging microscopy (OIM) system. The EBSD mappings were obtained with step sizes of 250 nm and 50 nm for the samples rolled to strains of 0.4 and 1.2–4.0, respectively. The OIM images were subjected to clean up procedure setting a minimal confidence index of 0.1. The volume fraction of α' – martensite was averaged through OIM, X-Ray diffraction and magnetic force microscopy. An average grain size was measured perpendicular to the rolling direction by a linear intercept method counting all high-angle boundaries with misorientations of $\theta \geq 15°$ revealed by OIM micrographs. The dislocation density was evaluated by means of kernel average misorientation (θ_{KAM}) as $\rho = 1.54\ \theta_{KAM}/(b\ h)$, where b and h are the Burgers vector and the EBSD step size, respectively.[21] The first nearest neighbors (1st neighbor rank) without any predefined threshold misorientations were used for the θ_{KAM} calculations. The mechanical properties of the cold rolled steels were determined by tensile tests at room temperature using an Instron 5882 testing machine with a crosshead speed of 2 mm/min. Depending on the sample dimensions, the tensile specimens with gauge lengths (L) of 5.65 mm to 21 mm (rectangular cross section areas (S) of 1 mm^2 to 14 mm^2, respectively, to provide the relationship of $L = 5.65\sqrt{S}$) were prepared by an electric-discharge method. The tensile axis was parallel to the rolling direction.

3. Results and Discussion

3.1. Deformation Microstructures and Internal Stresses

The microstructural evolution in an S304H-type austenitic stainless steel during cold rolling has been described in general elsewhere.[7] The present paper is concentrated on the detailed quantitative evaluation of deformation microstructures including dislocation substructures and corresponding internal distortions that develop at different strain levels in order to obtain an adequate structure-strength relationship. Typical deformation microstructures that develop in the present S304H austenitic stainless steel during cold bar rolling are shown in **Fig. 1**. Generally, the cold bar rolling is accompanied by the progressive refinement of the microstructure, finally leading to the development of lamellar grains with the transverse size of about 200 nm. The grain refinement during cold working is assisted by both the development of deformation twinning and the strain-induced martensitic transformation. The former frequently operates at relatively small strains, $0 < \varepsilon \leq 2$ (Figs. 1(a) and 1(b)), whereas the latter readily develops at sufficiently large strains, $\varepsilon \geq 1$ (Figs. 1(b) and 1(c)).

The strain effect on the volume fraction of martensite is shown in **Fig. 2**. The equilibrium ferrite fraction as calculated by ThermoCalc (TCFE6) for 300 K is also indicated in Fig. 2 by dashed line for reference. Cold rolling to relatively small strains is not accompanied by remarkable martensitic transformation; the martensite fraction does not exceed a few percent at strains below 0.5. In contrast, further straining accelerates the martensitic transformation. The martensite fraction rapidly increases to about 0.5 during cold rolling in the range of total true strains of $1 \leq \varepsilon \leq 2$. Then, the rate of strain-induced martensite development gradually decreases leading the martensite fraction to approach a saturation of about 0.8 at large strains. The strain-induced martensite appears at locally distorted regions, *i.e.*, microshear bands, deformation twins and, especially, their intersections.[7–9] Therefore, the martensite fraction (F_M) follows sigmoid shape with strain (ε) as predicted by Olson and Cohen,[22] *i.e.*,

$$F_M = 1 - \exp(-B(1 - \exp(-A\varepsilon))^n) \quad \text{..... (1)}$$

where B = 2, A = 0.5, n = 2.8, as indicated by solid line in Fig. 2.

Figure 3 shows the change in the transverse size of austenite and martensite grains during cold rolling. The transverse austenite grain size drastically reduces to 400 nm owing to the development of deformation twinning in the strain range of $0 < \varepsilon \leq 1$ followed by further gradual reduction to about 200 nm during subsequent rolling to a total strain of 4.0. The strain-induced martensite appears with an average grain size of about 350 nm at an early deformation. Similar to austenite, the transverse martensite grain size approaches 200 nm during cold rolling to a strain of 4.0. Assuming that the transverse grain size follows the change in cross section of rolled sample, the grain size can be represented by a liner function in semi-logarithmic coordinates (indicated by dashed line in Fig. 3). It is clearly seen in Fig. 3 that the transverse size of the grains decreases much faster than that of the whole sample in the range of relatively small strains below 1. In contrast, the reduction of the sample cross section predicts finer grain size in the range of rolling strains above 1. This suggests that the number of grains through the cross section of sample decreases during cold rolling to large total strains. Therefore, the grain refinement in the present study can be primarily attributed to the deformation twinning, whereas the strain-induced martensitic transformation does not contribute to the grain refinement remarkably. The change in the grain size in large strains follows a common tendency, which is characterized by an apparent steady-state behavior, when the grain size becomes strain invariant as reported for various metallic materials subjected to large strain deformation.[23–25]

Generally, various metals and alloys subjected to severe plastic deformations are characterized by the development of high internal stresses, which are attributed to both the high dislocation density in ultrafine grain/subgrain interiors and the strain-induced grain/subgrain boundaries being in non-equilibrium state.[18,20,26–28] Following a rapid increase at an early stage of cold working, the interior dislocation density was shown to approach a saturation or reportedly even decreased at sufficiently large strains.[24,27] In contrast, the internal stresses were shown to gradually increase with straining as a result of increasing the internal distortions

© 2016 ISIJ

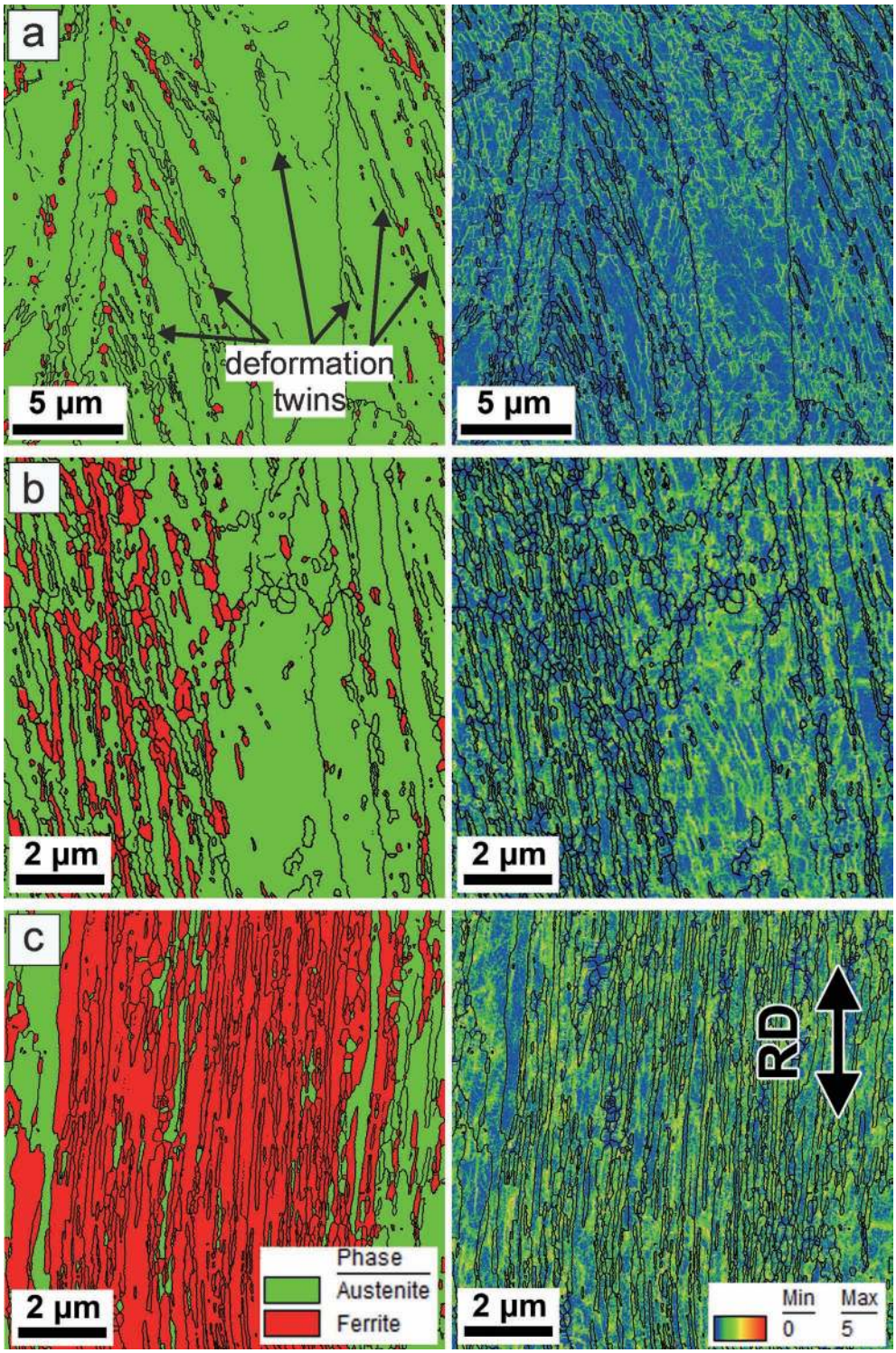

Fig. 1. Deformation microstructures developed in an S304H stainless steel during cold bar rolling to total strains of 1.2 (a), 2.0 (b) and 4 (c). The austenite (green) and martensite (red) distributions are shown in the left side pictures, and the corresponding kernel average misorientation distributions are represented in the right side figures. The grain/phase boundaries are indicated by black lines. (Online version in color.)

including those caused by strain-induced (sub) boundaries.[28] Therefore, the internal distortions should be taken into account to evaluate the structural/substructural strengthening by large strain cold working. The kernel average misorientation (KAM) seems to be the most appropriate parameter for quantitative estimation of the internal distortions,[29] because KAM represents overall distortions irrespective of their dislocation or (sub) boundary origin. The transverse subgrain size of about 50 nm in the samples rolled to strains of 1.2–4.0 was revealed by previous transmission electron microscopy investigation.[7] Internal lattice distortions in largely strained materials can be mutually screened by neighbor dislocation/cell subboundaries, leading to oscillation of local lattice curvatures between two points with an increase in the distance between the points.[28,30,31] Since the neighbor subboundaries may have opposite misorientations, the step size in KAM maps should not exceed the transverse subgrain size, otherwise the local distortions and

© 2016 ISIJ

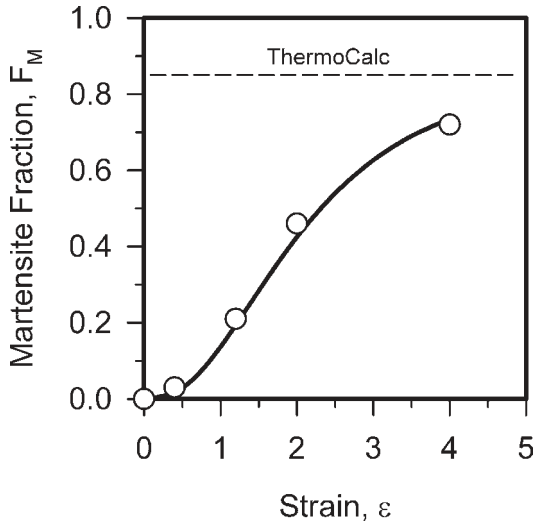

Fig. 2. Effect of the cold rolling strain on the martensite fraction in an S304H stainless steel.

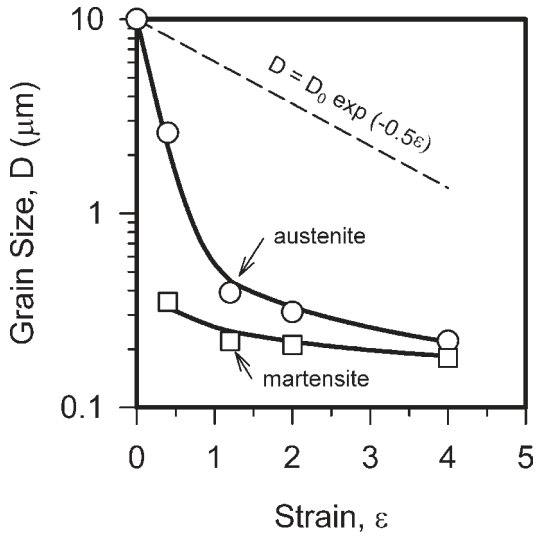

Fig. 3. Effect of the cold rolling strain on the transverse austenite (circles) and martensite (squares) grain size in an S304H stainless steel.

corresponding dislocation densities will be underestimated. On the other hand, the effect of EBSD processing accuracy on the estimation of internal stresses by means of local curvature between two points should drastically increase with a decrease in the step size. (In fact, the local stress will go to infinity as the distance between the points decreases to zero, assuming a constant error in the EBSD processing). Therefore, the step size of OIM maps of 50 nm was selected in the present study for the samples strained to 1.2–4.0 in order to evaluate the internal distortions and corresponding dislocation densities.

The OIM images displaying the KAM distributions in the cold rolled samples are shown in Fig. 1 (right side pictures). It is clearly seen in Fig. 1 that the KAM values increase as the cold rolling strain increases. The corresponding dislocation densities in the austenite and strain-induced martensite as estimated by means of KAM are shown in **Fig. 4**. The dislocation density measured by TEM[7] is also displayed in Fig. 4 by dotted line for a reference. The both KAM and

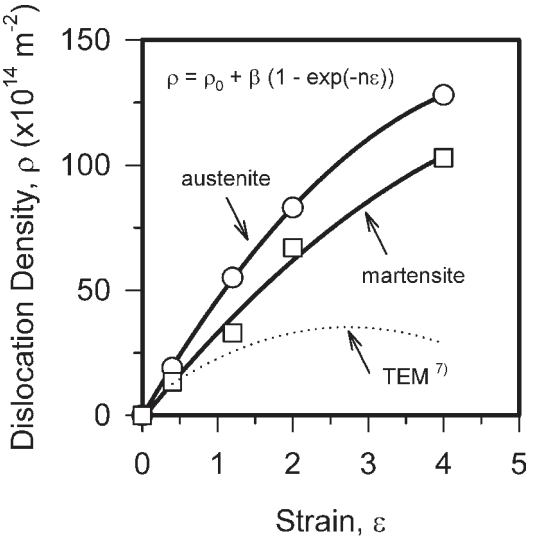

Fig. 4. Increase in the dislocation density in austenite and strain-induced martensite grains during cold rolling of an S304H stainless steel.

TEM give almost the same values of dislocation densities evolved at relatively small strains. In contrast, the dislocation density estimated by KAM is remarkably higher than that evaluated by TEM in the largely strained samples, and this difference increases with an increase in the total strain. The relatively low dislocation density as obtained by TEM is associated with local counting of individual dislocations in grain/subgrain interiors only. The KAM method gives the dislocation density, which is responsible for the measured lattice curvature. In this case the obtained dislocation density can be considered as a unique source of internal stresses. It has been suggested that the change in the dislocation density during cold working can be expressed by an exponential function of true strain,[32] *i.e.*,

$$\rho = \rho_0 + \beta(1-\exp(-n\varepsilon)) \quad \text{..... (2)}$$

Where ρ_0 is approximately 10^{12} m^{-2}.[9] The best fit of experimental results (solid lines in Fig. 4) is obtained with $\beta = 20\times10^{15}$ m^{-2}, n = 0.25 for austenite and $\beta = 16\times10^{15}$ m^{-2}, n = 0.25 for strain-induced martensite. The dislocation density in austenite and martensite increases during cold rolling in similar manner, although the strain-induced martensite is characterized by somewhat lower dislocation density than the austenite. This difference in dislocation density can be associated with enhanced dislocation mobility and recovery in ferritic grains.[33] The dislocation density almost linearly increases with strain in the range of $0 < \varepsilon \leq 2$, resulting in $\rho = 8\times10^{15}$ m^{-2} and $\rho = 6\times10^{15}$ m^{-2} in austenite and martensite, respectively. Then, the rate of dislocation accumulation decreases upon further processing. Finally, the dislocation density approaches 13×10^{15} m^{-2} in austenite and 10×10^{15} m^{-2} in martensite after cold rolling to a large total strain of 4. Such high dislocation densities and corresponding internal distortions should affect significantly the mechanical properties of the cold rolled steel. The transverse grain size and dislocation density evolved in the cold rolled samples are listed in **Table 1**.

© 2016 ISIJ

Table 1. Transverse grain size and dislocation density evolved in austenite and martensite of a cold rolled S304H stainless steel.

Cold strain	Grain size, nm		Dislocation density, 10^{15} m^{-2}	
	austenite	martensite	austenite	martensite
$\varepsilon = 0$	10 000±1 000	–	0.001	–
$\varepsilon = 0.4$	2 610±250	350±50	1.9	1.4
$\varepsilon = 1.2$	390±40	220±25	5.5	3.3
$\varepsilon = 2$	310±30	210±20	8.3	6.7
$\varepsilon = 4$	220±30	180±20	12.8	10.3

3.2. Tensile Behavior

A series of typical stress – strain curves for the samples processed by cold bar rolling to various total strains of 0.4 to 4 is shown in **Fig. 5**. The stress – strain curve for the initial state (hot rolling with subsequent annealing at 1 373 K) is also depicted in Fig. 5 for reference. In the initial state, the steel is characterized by large elongation to rupture of approximately 60% and a low value of yield strength of about 295 MPa. Such mechanical properties, *i.e.* low strength compromised by enhanced ductility, are inherent in recrystallized microstructures that evolved by high temperature annealing. After cold rolling to a total strain of 0.4, the yield strength increases almost threefold to 1 010 MPa. The strengthening during cold working can be attributed to the evolution of high dislocation density along with the grain subdivision by deformation twinning and strain-induced martensitic transformation. The yield strength continuously increases as the rolling strain increases and reaches above 2 000 MPa at a total strain of 4. In contrast to the strength, the elongation to rupture demonstrates inverse dependence on the rolling strain. After cold rolling to a strain of 4, the elongation to rupture decreases to approximately 4%. It should be noted, however, that the cold rolled samples exhibit rather large reductions in area above 25% in spite of small total elongation. The mechanical properties that obtained by tensile tests are summarized in **Table 2**.

The significant strengthening at an early stage of cold rolling is clearly correlates with an increase in dislocation density and a rapid grain refinement. An early deformation brings about the evolution of high density of dislocation subboundaries and the development of multiple deformation twinning that results in rapid grain subdivision. On the other hand, the average transverse grain size remains almost constant in the strain range of 1.0–4.0. Therefore, the progressive strengthening in large strains can be associated with the evolution of large internal distortions resulting in high internal stresses. Let us consider the structural strengthening mechanisms in more detail.

3.3. Strengthening Mechanisms

The present steel subjected to cold rolling is characterized by two-phase structure, *i.e.*, austenite and strain-induced martensite. The yield strength of this two-phase steel ($\sigma_{0.2}$), therefore, can be expressed by a summation of the austenite ($\sigma_{0.2A}$) and martenite ($\sigma_{0.2M}$) strength:

$$\sigma_{0.2} = F_A\sigma_{0.2A} + F_M\sigma_{0.2M} \quad \text{..... (3)}$$

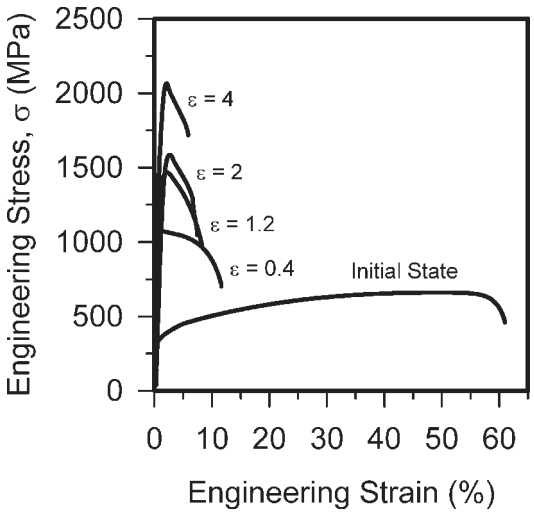

Fig. 5. Engineering stress – strain curves of an S304H stainless steel processed by cold bar rolling to various total strains (ε).

Table 2. Tensile properties of an S304H austenitic stainless steel subjected to cold bar rolling to various total strains.

Cold strain	Yield strength, MPa	Ultimate tensile strength, MPa	Elongation, %	Reduction in area, %
$\varepsilon = 0$	295±15	680±20	61±5	68±12
$\varepsilon = 0.4$	1 010±25	1 070±25	12±3	53±10
$\varepsilon = 1.2$	1 380±50	1 465±45	8±2	52±10
$\varepsilon = 2$	1 510±75	1 585±75	6±2	47±8
$\varepsilon = 4$	2 050±50	2 065±50	5±2	27±5

Where F_A and F_M are the austenite and martensite fractions ($F_A + F_M = 1$). Severe plastic deformations commonly result in the evolution of high dislocation density and numerous strain-induced grain boundaries. The grain subdivision by newly formed boundaries reduces the effective grain size. Thus, the strengthening due to reduced grain size (D) can be simply expressed by Hall-Petch relationship:[34–36]

$$\sigma_{0.2} - \sigma_0 = F_A K_A D_A^{-0.5} + F_M K_M D_M^{-0.5} \quad \text{..... (4)}$$

Where σ_0 is the strength of the sample with infinite grain size, K is a constant, index of A or M indicates austenite or martensite, respectively. Alternatively, the strengthening by cold working is frequently related to the increased dislocation density (ρ).[37–39] The dislocation strengthening in the present case can be expressed as follows:

$$\sigma_{0.2} - \sigma_0 = F_A\alpha_A G_A b_A \rho_A^{0.5} + F_M\alpha_M G_M b_M \rho_M^{0.5} \quad \text{.... (5)}$$

Where α is a product of a numerical factor and Tailor factor ($\alpha = \alpha^*$ M), G and b are the shear modulus and Burgers vector, respectively. Also, the strengthening by large strain deformations has been considered as a result of both mechanisms, *i.e.*, the grain size and dislocation strengthening, assuming that these mechanisms are independent and linearly additive.[9,40–42] It should be noted for the last case, however, that the reported grain size strengthening coefficients (K) were remarkably smaller than that in classical Hall-Petch relationship for metallic materials with recrystallized microstructure.[7,19,32,43–46] For instance, K = 0.435 MPa

© 2016 ISIJ

$m^{0.5}$ and K = 0.06 MPa $m^{0.5}$ were reported for grain size strengthening of recrystallized austenite[46] and concurrent grain size and dislocation strengthening of work hardened austenite,[45] respectively. As a result, the strength contribution from dislocation strengthening was apparently much larger than that from grain size strengthening. This might be associated with more complicated relationship between different strengthening mechanisms than assumed linearly additivity. Nevertheless, the dislocation strengthening was considered as a major contributor to the overall strength.

The plots of experimental strengthening in accordance with Eqs. (4) and (5) are shown in **Figs. 6** and **7**, respectively. Here, the same G = 81 000 MPa and $b = 2.5\times10^{-10}$ m were taken for austenite and martensite,[47] and σ_0 = 200 MPa as reported in numerous studies on chromium-nickel stainless steels.[7,9,44,48] It is clearly seen in Fig. 6 that the relationship between the strengthening and the austenite/martensite grain size is characterized by a complex non-monotonous dependence, which is hard to be extrapolated by a simple plane function. The least square method formally predicts the best fit of Eq. (4) with K_A = 0.7 MPa $m^{0.5}$ and K_M = 0.8 MPa $m^{0.5}$. Note here that these values of grain size strengthening coefficient remarkably exceed those reported for Hall-Petch equations, *i.e.* 0.3–0.5 MPa $m^{0.5}$ for austenite[7,19,37,46] and 0.2–0.7 MPa $m^{0.5}$ for ferrite.[49] In the latter case, the maximal value of strengthening coefficient corresponds to upper saturation limit for steels with large interstitial content.[49] In contrast to the grain size strengthening (Eq. (4) and Fig. 6), the relationship between the strengthening and the dislocation densities in austenite and martensite through Eq. (5) can be adequately represented by a unique plane function as shown in Fig. 7. It should be noted that the present rolling did not lead to remarkable change in the Tailor factor, which slightly increased from 3.0 in the original sample to 3.15 in austenite and 3.17 in martensite after rolling to a strain of 4 as revealed by OIM mapping, irrespective of apparently strong deformation textures inherent in unidirectional cold rolling. Therefore, the Tailor factor of M = 3 was taken in the calculation for a sake of simplicity. The best fit of experimental data through Eq. (5) is obtained with α_A = 0.79 and α_M = 0.85. It is worth noting that almost the same numerical factors (α) of 0.7 to 1.0 have been reported in other studies on dislocation strengthening.[9,32,44,50,51] In the case of concurrent operation of the grain size and dislocation strengthening, the following coefficients are obtained by the least square method, K_A = 0.2 MPa $m^{0.5}$, K_M = 0.02 MPa $m^{0.5}$, α_A = 0.77, α_M = 0.7. Here, the reasonable values are obtained for the dislocation strengthening factors (α), whereas the grain size strengthening coefficients, especially K_M, are relatively small.

The relationships between the experimental values of yield strength and those calculated for the grain size strengthening ($\sigma_{0.2}$(D)) by Eq. (4), or the dislocation strengthening ($\sigma_{0.2}(\rho)$) by Eq. (5), or both grain size and dislocation strengthening ($\sigma_{0.2}$(D+ρ)) are shown in **Fig. 8**.

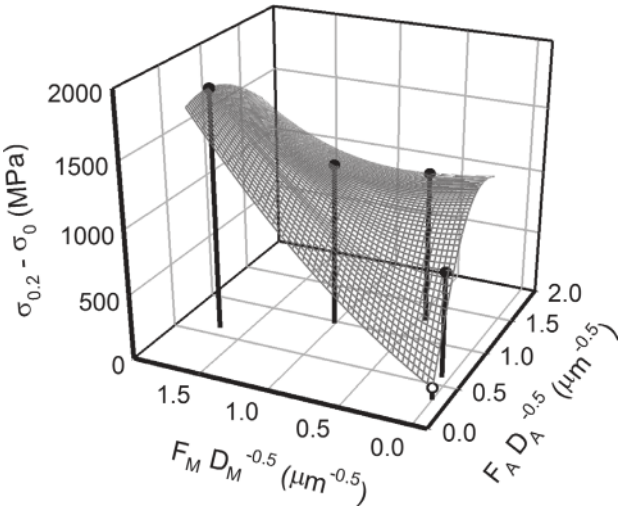

Fig. 6. Relationship between the strengthening and inverse square root of the boundary spacing of austenite and martenite for an S304H stainless steel subjected to cold rolling. The data point of original sample is shown by open symbol.

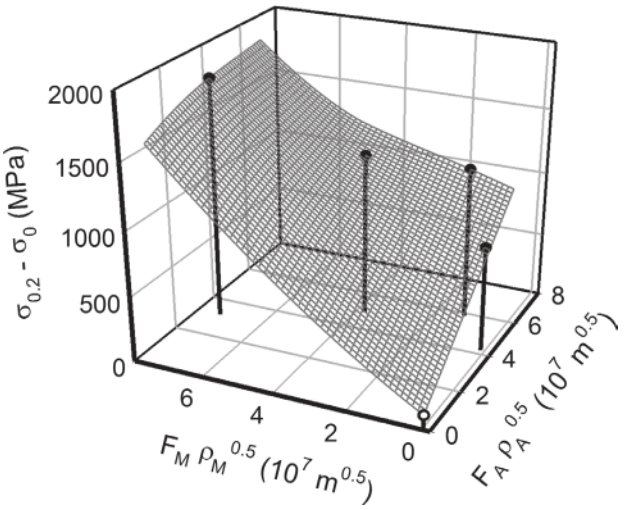

Fig. 7. Relationship between the strengthening and the square root of dislocation density in austenite and martensite for an S304H stainless steel subjected to cold rolling. The data point of original sample is shown by open symbol.

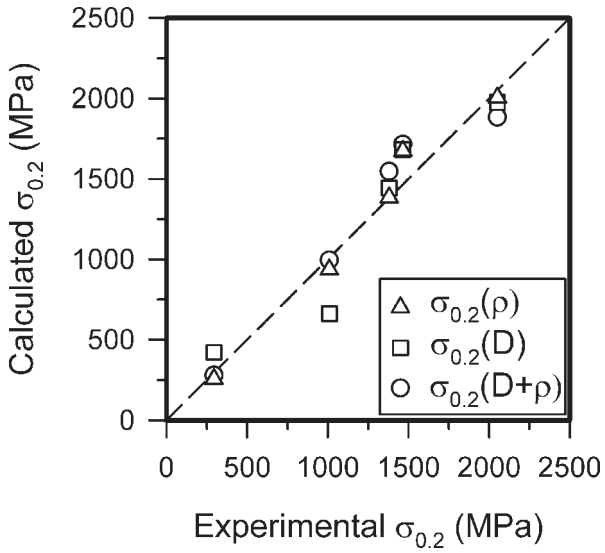

Fig. 8. Relationship between the experimental yield strength and that calculated for dislocation strengthening ($\sigma_{0.2}(\rho)$), grain size strengthening ($\sigma_{0.2}$(D)), or both dislocation and grain size strengthening ($\sigma_{0.2}$(D+ρ)).

© 2016 ISIJ

It is clearly seen in Fig. 8 that the dislocation strengthening mechanism is the closest while the grain size strengthening mechanism is the worst approach for prediction of yield strength of the cold rolled stainless steel. Simultaneous consideration of dislocation and grain boundary strengthening also results in good correlation between the experimental and calculated values (Fig. 8), although the dislocation strengthening dominates over the grain size strengthening in this case. Therefore, the strengthening of the present stainless steel subjected to large strain cold rolling can be considered as dislocation strengthening. Such approach can be used to predict the strain hardening during cold working as illustrated in **Fig. 9** where the experimental flow stresses and those corresponding to dislocation strengthening are plotted versus total true strain.

Let us consider the change in the strength contribution from austenite and martensite in the present stainless steel during cold bar rolling in the framework of the dislocation strengthening that described above (**Fig. 10**). Following a rapid strengthening at an early cold deformation the austenite strength contribution gradually approaches a maximum at a total strain of about 1 and then steadily decreases with increasing the total rolling strain. The decrease in the austenite strength contribution to overall yield stress during cold rolling to strains above 1 is evidently associated with decrease in the austenite fraction because of strain-induced martensitic transformation. Correspondingly, the martensite strength contribution upon cold rolling follows the curve of martensitic transformation (cf. Figs. 2 and 10). It is interesting to note that the yield stresses of austenite and martensite that normalized by their fractions are quite similar to each other (shown by dashed lines in Fig. 10) and are almost the same with the overall yield strength (Fig. 9) in the studied range of rolling strains. Therefore, the austenite and strain-induced martensite in the stainless steel are identical in the dislocation strain hardening during cold rolling and provide equal fractional contribution to overall strengthening.

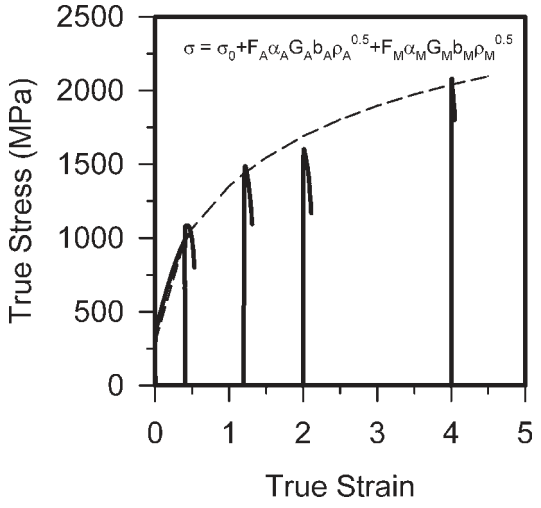

Fig. 9. Relationship between true strain and true stress obtained by tensile tests of an S304 stainless steel previously cold rolled to different total strains. The experimental and calculated data are shown by solid and dashed lines, respectively.

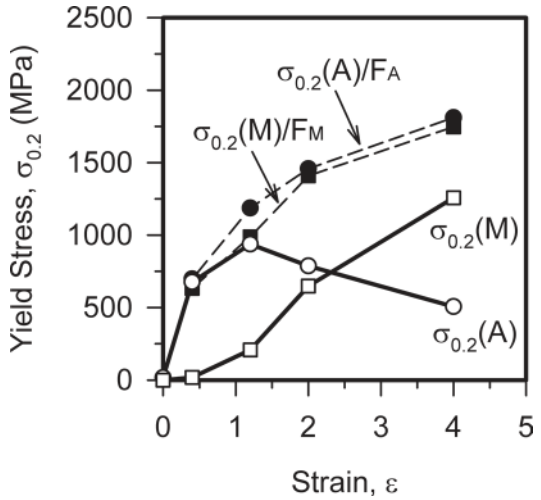

Fig. 10. Strength contribution from austenite and martensite to the yield stress of an S304H stainless steel during cold rolling.

4. Conclusions

The influence of large strain cold rolling on the mechanical properties of an S304H stainless steel was studied. The main results are summarized below.

(1) Cold rolling was accompanied by deformation twinning and strain-induced martensitic transformation, which resulted in rapid grain subdivision and the development of ribbon-type microstructure consisting of a mixture of highly elongated austenite and martensite grains with the transverse grain size of about 200 nm in the both phases.

(2) The deformation microstructures were characterized by high dislocation densities in both austenite and martensite grains. The change in the dislocation density during cold rolling that was evaluated by using kernel average misorientation from EBSP mapping can be expressed as

$$\rho = \rho_0 + \beta(1-\exp(-0.25\varepsilon))$$

where $\beta = 20\times10^{15}$ m^{-2} for austenite and $\beta = 16\times10^{15}$ m^{-2} for strain-induced martensite.

(3) Cold rolling resulted in significant strengthening. The yield strength progressively increased with an increase in the total rolling strain, approaching 2 050 MPa after rolling to a total strain of 4. The strengthening during cold rolling was attributed to the increasing dislocation density. The obtained results suggested the following relationship between the strengthening ($\sigma_{0.2} - \sigma_0$) and dislocation density in austenite (ρ_A) and martensite (ρ_M).

$$\sigma_{0.2} - \sigma_0 = F_A\alpha_A G_A b_A \rho_A^{0.5} + F_M\alpha_M G_M b_M \rho_M^{0.5}$$

where F_A, G_A, b_A and F_M, G_M, b_M are the phase fraction, the shear modulus, the Burgers vector in austenite and martensite, respectively, and $\alpha_A = 0.79$, $\alpha_M = 0.85$. This suggests that the austenite and strain-induced martensite experienced the same strengthening during cold rolling and provided equal fractional contribution to overall strength.

Acknowledgments

The financial support received from the Ministry of Education and Science, Russia, under grant No. 14.575.21.0070 (ID No. RFMEFI57514X0070) is greatly acknowledged. The authors are grateful to the personnel of the Joint

© 2016 ISIJ

Research Centre, Belgorod State University, for their assistance with instrumental analysis.

REFERENCES

1) K. H. Lo, C. H. Shek and J. K. L. Lai: *Mater. Sci. Eng. R*, **65** (2009), 39.
2) W. Martienssen and H. Warlimont: Springer Handbook of Condensed Matter and Materials Data, Springer, Berlin, (2005), 240.
3) R. Ishibashi, H. Arakawa, T. Abe and Y. Aono: *ISIJ Int.*, **40** (2000), S169.
4) Y. Nakao and H. Miura: *Mater. Sci. Eng. A*, **528** (2010), 1310.
5) H. Ueno, K. Kakihata, Y. Kaneko, S. Hashimoto and A. Vinogradov: *J. Mater. Sci.*, **46** (2011), 4276.
6) S. V. Dobatkin, V. F. Terentev, W. Skrotzki, O. V. Rybalchenko, M. N. Pankova, D. V. Prosvirnin and E. V. Zolotarev: *Russ. Metall.* (*Metally*), **2012** (2012), 954.
7) I. Shakhova, V. Dudko, A. Belyakov, K. Tsuzaki and R. Kaibyshev: *Mater. Sci. Eng. A*, **545** (2012), 176.
8) A. Belyakov, M. Odnobokova, A. Kipelova, K. Tsuzaki and R. Kaibyshev: *IOP Conf. Series: Mater. Sci. Eng.*, **63** (2014), paper No. 012156.
9) M. Odnobokova, A. Belyakov and R. Kaibyshev: *Metals*, **5** (2015), 656.
10) R. E. Schramm and R. P. Reed: *Metall. Trans. A*, **6A** (1975), 1345.
11) J. Talonen and H. Hanninen: *Acta Mater.*, **55** (2007), 6108.
12) T.-H. Lee, E. Shin, C.-S. Oh, H.-Y. Ha and S.-J. Kim: *Acta Mater.*, **58** (2010), 3173.
13) T.-H. Lee, C.-S. Oh and S.-J. Kim: *Scr. Mater.*, **58** (2008), 110.
14) N. Nakada, H. Ito, Y. Matsuoka, T. Tsuchiyama and S. Takaki: *Acta Mater.*, **58** (2010), 895.
15) N. Tsuchida, Y. Morimoto, T. Tonan, Y. Shibata, K. Fukaura and R. Ueji: *ISIJ Int.*, **51** (2011), 124.
16) N. Tsuji and T. Maki: *Scr. Mater.*, **60** (2009), 1044.
17) F. Forousan, A. Najafizadeh, A. Kermanpur, A. Hedayati and R. Surkialiabad: *Mater. Sci. Eng. A*, **527** (2010), 7334.
18) M. M. Abramova, N. A. Enikeev, R. Z. Valiev, A. Etienne, B. Radiguet, Y. Ivanisenko and X. Sauvage: *Mater. Lett.*, **136** (2014), 349.
19) C. X. Huang, G. Yang, C. Wang, Z. F. Zhang and S. D. Wu: *Metall. Mater. Trans. A*, **42A** (2011), 2061.
20) H. Wang, I. Shuro, M. Umemoto, H.-H. Kuo and Y. Todaka: *Mater. Sci. Eng. A*, **556** (2012), 906.
21) A. P. Zhilyaev, I. Shakhova, A. Belyakov, R. Kaibyshev and T. G. Langdon: *Wear*, **305** (2013), 89.
22) G. B. Olson and M. Cohen: *Metall. Trans. A*, **6A** (1975), 791.
23) F. J. Humphreys, P. B. Prangell, J. R. Bowen, A. Gholinia and C. Harris: *Philos. Trans. R. Soc. Lond. A*, **357** (1999), 1663.
24) A. Belyakov, K. Tsuzaki and Y. Kimura: *ISIJ Int.*, **48** (2008), 1071.
25) R. Pippan, S. Scheriau, A. Taylor, M. Hafok, A. Hohenwarter and A. Bachmaier: *Annu. Rev. Mater. Res.*, **40** (2010), 319.
26) R. Z. Valiev, R. K. Islamgaliev and I. V. Alexandrov: *Prog. Mater. Sci.*, **45** (2000), 103.
27) A. Belyakov, T. Sakai, H. Miura and R. Kaibyshev: *Philos. Mag. Lett.*, **80** (2000), 711.
28) A. Belyakov, Y. Kimura, Y. Adachi and K. Tsuzaki: *Mater. Trans.*, **45** (2004), 2812.
29) M. Calcagnotto, D. Ponge, E. Demir and D. Raabe: *Mater. Sci. Eng. A*, **527** (2010), 2738.
30) A. E. Romanov and V. I. Vladimirov: Dislocation in Solids, Vol. 6, ed. by F. R. N. Nabarro, Elsevier Science, Amsterdam, The Netherlands, (1992), 191.
31) A. Belyakov, R. Kaibyshev and T. Sakai: *Metall. Mater. Trans. A*, **29A** (1998), 161.
32) P. Kusakin, A. Belyakov, R. Kaibyshev and D. Molodov: *IOP Conf. Series: Mater. Sci. Eng.*, **63** (2014), paper No. 012059.
33) A. Belyakov, Y. Kimura and K. Tsuzaki: *Acta Mater.*, **54** (2006), 2521.
34) E. O. Hall: *Proc. Phys. Soc. B*, **64** (1951), 747.
35) R. Armstrong, I. Codd, R. M. Douthwaite and N. J. Petch: *Philos. Mag.*, **7** (1962), 45.
36) R. W. Armstrong and P. Rodriguez: *Philos. Mag.*, **86** (2006), 5787.
37) G. Langford and M. Cohen: *Trans. ASM*, **62** (1969), 623.
38) H. Mecking and U. F. Kocks: *Acta Metall.*, **29** (1981), 1865.
39) Y. Estrin, L. S. Toth, A. Molinari and Y. Brechet: *Acta Mater.*, **46** (1998), 5509.
40) D. A. Hughes and N. Hansen: *Acta Mater.*, **48** (2000), 2985.
41) N. Hansen: *Scr. Mater.*, **51** (2004), 801.
42) R. Z. Valiev: *Mater. Trans.*, **55** (2014), 13.
43) B. P. Kashyap and K. Tangri: *Scr. Metall.*, **24** (1990), 1777.
44) Z. Yanushkevich, A. Mogucheva, M. Tikhonova, A. Belyakov and R. Kaibyshev: *Mater. Charact.*, **62** (2011), 432.
45) Z. Yanushkevich, A. Belyakov, C. Haase, D. A. Molodov and R. Kaibyshev: *Mater. Sci. Eng. A*, **651** (2016), 763.
46) Z. Yanushkevich, A. Belyakov, R. Kaibyshev, C. Haase and D. A. Molodov: *Mater. Charact.*, **112** (2016), 180.
47) H. J. Frost and M. F. Ashby: Deformation Mechanism Maps, Pergamon Press, Oxford, UK, (1982), 62.
48) C. M. Young and O. D. Sherby: *J. Iron Steel Inst.*, **211** (1973), 640.
49) S. Takaki, D. Akama, N. Nakada and T. Tsuchiyama: *Mater. Trans.*, **55** (2014), 28.
50) X. Huang, S. Morito, N. Hansen and T. Maki: *Metall. Mater. Trans. A*, **43A** (2012), 3517.
51) T. J. Harrell, T. D. Topping, H. Wen, T. Hu, J. M. Schoenung and E. J. Lavernia: *Metall. Mater. Trans. A*, **45A** (2014), 6329.

© 2016 ISIJ